Journal of *Marine Science and Engineering*

MDPI

Article

Finite Element Analysis of the Effect of Currents on the Dynamics of a Moored Flexible Cylindrical Net Cage

Zhongchi Liu, Sarat Chandra Mohapatra and C. Guedes Soares *

Centre for Marine Technology and Ocean Engineering (CENTEC), Instituto Superior Técnico, Universidade de Lisboa, Av. Rovisco Pais 1, 1049-001 Lisboa, Portugal; zhongchi.liu@centec.tecnico.ulisboa.pt (Z.L.); sarat.mohapatra@centec.tecnico.ulisboa.pt (S.C.M.)
* Correspondence: c.guedes.soares@centec.tecnico.ulisboa.pt

Abstract: A numerical model associated with wave–current interactions with a moored flexible cylindrical cage was developed based on the finite element method. An analytical model was formulated under the linearised wave theory and small structural response, and a semi-analytical solution was obtained using the Fourier Bessel series solution and least squares approximation method, along with a matching technique. The numerical results from the finite element analysis of the horizontal displacements for different design parameters under a uniform current were compared with the analytical model solutions. It was seen that they had a good level of agreement with their results. The effects of different current speeds and time on the cage shapes were analysed from the finite element results. Further, the mooring forces on the flexible cage for different values of the cage height and cage radius were also presented. The comparison of the results indicated that the numerical model results could be used with confidence in the design of a flexible cylindrical net cage for applications to offshore aquacultures.

Keywords: cylindrical net cage; current; mooring lines; least squares approximation method; finite element analysis

Citation: Liu, Z.; Mohapatra, S.C.; Guedes Soares, C. Finite Element Analysis of the Effect of Currents on the Dynamics of a Moored Flexible Cylindrical Net Cage. *J. Mar. Sci. Eng.* **2021**, *9*, 159. https://doi.org/10.3390/jmse9020159

Academic Editor: Alejandro J. C. Crespo
Received: 23 January 2021
Accepted: 1 February 2021
Published: 5 February 2021

1. Introduction

Due to the decreasing of fish stocks and the increased need of aquacultures, there is a need to further develop aquacultures offshore. Therefore, models that allow the analysis of floating flexible net-type fish cages with a mooring system under the effects of waves and the current are very important. These floating flexible net-type fish cages are economically important, as they are meant not to suffer structural failures during storm events. In order to model a floating flexible net-type fish cage, the dynamic response and structural analysis are of great importance to ensure the safety of the flexible marine cages. Particularly, designing floating net cages and mooring systems [1,2] is of great concern to the marine aquaculture industry. The consideration of current loading on the dynamic response of aquaculture cages is necessary when designing fish farms, enabling the estimation of operational limits of a particular design system component [3].

In recent years, there has been significant progress in the study of various aspects of wave propagation through net cages and hydrodynamic loading of the cages, based on different software and numerical methods. Some of the previous studies are discussed below.

In order to get enough aquaculture space and keep away from the pollution in the inshore area, fish farms are moving to offshore regions where high-velocity currents can provide enough oxygen and take away waste production [4,5]. A mass-spring model was used in [6] to build a computation model of a fish cage and a pound net. A strength analysis of aquaculture net cages under currents from 0.1 to 0.5 m/s was performed in [7], and it was identified that the forces on the bottom panels could reach the design capacity.

Based on both experimental and numerical models, the deformation of the cage with different solidities was studied in [8]. Pressure sensors were used to measure the

instantaneous position of several points on the cages at two Atlantic salmon farms in Norway and the Faroe Islands, and the volume of the cage was estimated using the geometry formed by the measured points in [9]. Further, the acoustic sensors were used to measure both the vertical and horizontal position of the net and calculate the deformation of a small-scale gravity cage in [10]. The drag forces and deformation of the fish cages were measured and calculated based on full towing tests in the field at different speeds, and they indicated that there was a need for a better description of the flow past net cages in [11].

Shell elements were used to simulate the high-density polyethylene (HDPE) floating collar and find the stress concentration locations on the collar in [12], and further, they used the finite element analysis (FEA) results to derive the fatigue life. A numerical model of a 10-cage fish farm was developed to compute the mooring forces in [13].

To obtain the added mass and drag coefficients in the Morison Equation, forced oscillation tests were conducted to simulate the water particle motions around a hollow cylinder in waves and the results were applied in their FEA model in [14]. In order to apply the buoyant load correctly, a "Buoyancy Distribution" method was developed using parallel beam elements to model the collar [15]. The comparison of different models of the net with the experimental results was made in [16] and concluded that these models can calculate the hydrodynamic load under currents slower than 0.5 m/s accurately but overestimate the drag forces under large currents. A FEA model was developed in [17] to study the arrangement of the cross ropes and bottom ropes on the net and decrease the stress concentration during lifting. The wake effect on flexible aquaculture nets with porous natures and in their FEA model by FhSim was studied in [18].

An interesting feature of these problems is the study of mooring lines and deformation of the fish cage under the actions of waves and currents. For instance, the influence on the fish farm mooring behaviour in different sea states using numerical computational fluid dynamics (CFD) model simulations were studied in [19]. In two-dimensional Cartesian coordinates, under steady currents and floater oscillations, the hydroelastic response of full-scale floater-and-net systems was investigated in [20]. Recently, a numerical framework for modelling open sea aquacultures in waves and currents based on CFD was developed to study the structural dynamics of the net [21]. Solidity was defined as the ratio of the projected area to the circumscribed area of the net, which is an essential parameter and determines the projected area. The hydrodynamic loads acting on high solidity net cage models under high uniform flow velocities and deformation of the net cage based on model tests and standard Morison-type numerical analyses was investigated in [8].

Further, the analysis of net cages under the combined effect of waves and currents was performed based on numerical and experimental studies. The nonlinear wave-induced motions of floating cylindrical-shaped floaters of fish farms based on the model test and numerical simulations based on a CIP (Carbon-in-Pulp)-based numerical wave tank (NWT) was addressed in [22]. The influence of fish on the mooring loads of a floating net cage based on numerical and experimental methodologies was studied in [1]. The mooring loads of a circular net cage with an elastic floater in the waves and currents were investigated in [23]. An improved screen type force model and the truss model were used to calculate viscous current and wave loads on aquaculture nets in [24]. The mooring loads on an aquaculture net cage in currents and waves were investigated based on a model test and numerical simulations where the model tests were performed to provide benchmark data in [25]. A realistic aquaculture fish farm in both regular and irregular waves based on numerical simulations and experimental tests and the mooring loads in the front two anchor lines and bridle lines were analysed in [2].

The behaviour of traditional-type fish farms with net cages and closed fish farms in waves and currents was discussed in [3]. The effects of waves and currents on the behaviour of a gravity-type cage system were investigated in [26], which used a tube-sinker to replace the common weights at the bottom of net cages to overcome the deformation. The hydrodynamic behaviour of a submergible net cage and mooring system under the actions of waves and currents was analysed in [27]. The results were compared between

numerical simulations and physical models in different cases. Then, the hydrodynamic behaviours of multiple net cages and submerged mooring grid systems under waves and current flow were analysed in [28] by performing numerical simulations and a series of experiments. A 3D series of measurements of a large sea cage volume deformation and current flow around and within the cage based on experiments and numerical simulations was analysed in [29]. A numerical model was developed to investigate the deformations and stress distribution of the floating collar of a fish cage subjected to the flow in a steady current, and the modelling approach was based on the combination of the finite element method using the shell element to simulate the floating pipes [30].

The eigenfunction matching technique has been widely used in the problems of surface wave interactions with floating and submerged flexible structures. The technique has gained wide popularity due to its considerable accuracy and less use of computer memory and processing time. Some of the previous works associated with floating and submerged flexible structures using the eigenfunction matching technique are discussed below, which are the mathematical basis for the current work. The effects of submerged flexible and horizontal flexible membranes on a moored floating elastic plate were based on a hydroelastic analysis using the eigenfunction expansion method [31]. Under three-dimensional Cartesian coordinates, the hydroelastic analysis of floating and submerged flexible plates based on the eigenfunction expansion method was investigated in [32]. Recently, the hydroelastic response of a submerged flexible porous plate was analysed based on the eigenfunction expansion method in [33]. An oblique wave interaction with a horizontal flexible porous membrane was investigated by applying the eigenfunction expansion method to analyse the wave energy dissipation of a porous membrane application to breakwater [34]. Further, a new composite breakwater of a submerged horizontal flexible porous membrane with a lower rubble mound was developed under the eigenfunction matching technique in [35].

On the other hand, the hydrodynamic response of a flexible fishnet cylinder was studied analytically under regular waves where the net was modelled as a porous flexible cylinder in finite water depth that deformed like a one-dimensional beam under the linearised water wave theory in [36]. Recently, a more extensive and detailed review of fish cage models based on analytical, numerical, and experimental methodologies was presented [37].

From the above literature, it was found that, until now, there was no comparison reported between the numerical finite element model (FEM) and analytical model results of a moored floating flexible cylindrical cage model exposed to a uniform current. Therefore, in the present paper, a FEA numerical model was developed to simulate a moored floating flexible cylindrical net cage under waves and a current. On the other hand, a mathematical model associated with the surface wave interaction with a moored floating flexible cylindrical net cage was formulated, subjected to a uniform current based on linearised potential flow theory, and a flexible cylindrical cage was modelled as a surface-piercing flexible porous cylinder having a flexible porous membrane-type bed.

Numerical simulations were performed based on the FEA model, whilst an analytical solution was obtained using the matched eigenfunction expansion and least squares approximation method. The FEA was able to simulate the dynamic behaviour of a net cage, whilst the numerical results of the analytical expressions were computed by developing a MATLAB code incorporating a numerical perturbation scheme and associated Bessel functions. The cage shapes for different current speeds and different times in a wave period were presented based on the numerical FEA model. Further, the axial loads on the mooring lines for different design parameters were analysed.

2. Finite Element Model Formulation and Description

2.1. Brief Description of Finite Eelement Model

A gravity fish cage is usually composed of four parts: a floating collar, containment nets, sinkers, and mooring lines [11]. The collar and sinkers are used to stretch the net and balance buoyancy and gravity. Mooring lines connect the collar and the seabed to fix the

position of the cage. Due to the slender structure, the collar should be modelled by pipe elements. Truss elements were used to simulate the bending behaviour of the flexible nets. Similar to the net, for the mooring lines, nonlinear springs with only tensile behaviours were used. Due to the large displacement of the net, the geometrical nonlinearity should be considered. The numerical model was built in the commercial software ANSYS/APDL, which was used to solve the dynamic motion equation. A more elaborate description of these components is as follows.

2.1.1. Collar

In a gravity cage, the collar is usually a hollow annular structure and is mainly used to provide buoyancy. Due to the slender and hollow structure, pipe elements are selected to model the collar, and elastic deflection due to bending was accounted for [38].

2.1.2. Flexible Net

In this FEA model, truss elements were used to simulate the net. The solidity, which is defined as the ratio between the projected area of the twines and the total area of a net mesh, is an important parameter and determines the projected area and hydrodynamic load on the structure. The solidity of the net is [39]

$$S_n = \frac{2d}{L} - \left(\frac{d}{L}\right)^2, \quad (1)$$

where S_n is the solidity of the net, d is the thickness of one twine, and L is the width of one mesh.

In this paper, 2 mm was chosen as the diameter of the net [11]. However, if truss elements with the same diameter as the net are used, the model will include too many elements to calculate. Thus, the net was simplified by horizontal and vertical bar elements with equivalent larger diameters. In this way, much fewer truss elements were used to form the structure. The total section area of the adjusted structure was same as the original structure. Additionally, to keep the same weight and tensile stiffness as the original structure, the density, the Young's modulus of the material, and the total cross-section area of the net were consistent with the original structure, which resulted in a smaller projected area under the current. In order to ensure that the hydrodynamic force consistent with the original structure, the drag and inertial coefficients were increased accordingly. Table 1 shows a set of the parameters of the adjusted net lines according to the diameters of the cage.

Table 1. Parameters of the truss elements.

	Adjusted Structure (D = 6 m)	**Adjusted Structure (D = 10 m)**
Single twine Diameter (mm)	2	2
No. of horizontal net lines	6	6
No. of vertical net lines	40	40
Diameter of horizontal net lines (mm)	17.68	17.68
Diameter of vertical net lines (mm)	11.24	14.51

2.1.3. Sinker

Sinkers are located at the bottom of the cage, and they stretch the net. The weight of the sinkers has a high influence on both the deformation of the cage and mooring forces [9]. In the model of this work, the sinker was formed by a solid bottom ring with a diameter of 0.1 m, and it was modelled by beam elements.

2.1.4. Mooring Lines

A mooring system is used to keep the motion of the fish cage within a certain range. Usually, a complete mooring system includes cables, ropes, and chains with buoys on them. In this work, the mooring system was simplified into two mooring lines. To simulate the flexible behaviour of the mooring lines under compression, nonlinear spring elements with only tensile stiffness were used. The layout of the two mooring lines is illustrated in Figure 1.

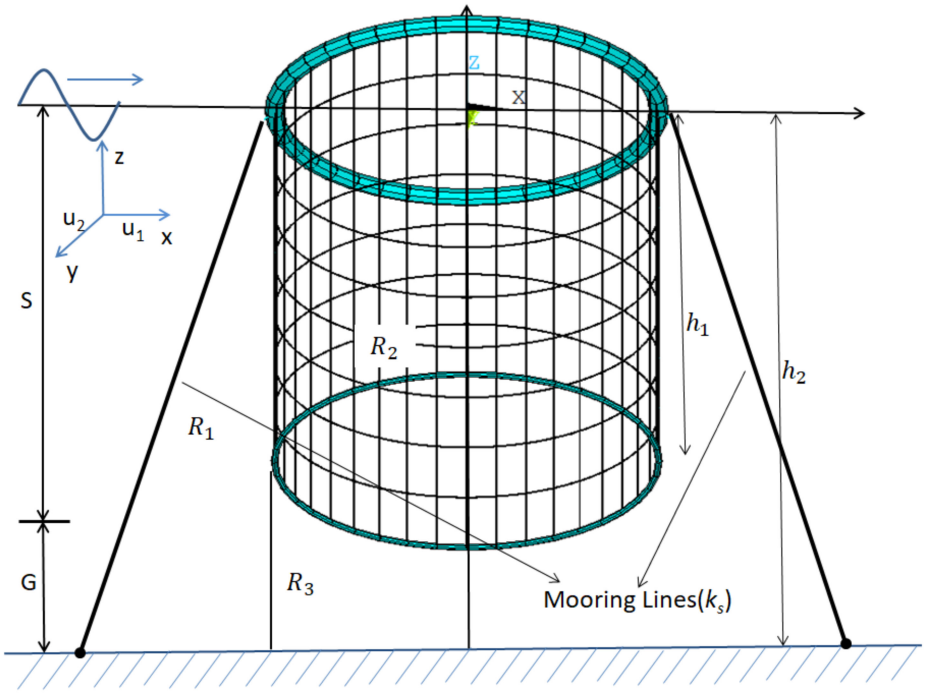

Figure 1. Moored (stiffness k_s) flexible cylindrical net cage under a uniform current u $(= u_1 = u_2)$.

2.2. Fluid Flow and Hydrodynamic Load

The dynamic response of the fish cage under both the current and waves was analysed in this paper. For the whole structure, the dynamic equation can be expressed as [15]

$$[M]\left[\ddot{x}\right] + [C]\left[\dot{x}\right] + [K][x] = G + f_b + f_H \tag{2}$$

where $[M]$ is the mass matrix, $[C]$ is the damping matrix, and $[K]$ is the stiffness matrix. Furthermore, G, f_b, and f_H are the load vectors, including gravity, buoyancy, and hydrodynamic load, respectively.

The direction of the current and waves is indicated in Figure 1. The current velocities varied from 0.2 m/s to 0.8 m/s. The linear wave theory was used to model the waves. The depth of the flow field was set as 500 m, which was much larger than the length of the waves. The velocity potential and dispersion relationship were expressed as Equations (3) and (4). Due to the slender structure of the collar and net, the Morison equation (Equation (5)) was used to calculate the hydrodynamic force. To take the relative motion between the structure and water particles into account, a modified Morison equation was expressed as Equation (6) [39]. A drag coefficient of C_D = 1.2 and an inertia coefficient of C_m = 2 were used in the simulation [40,41].

$$\phi(x,z,t) = \frac{Hg}{2\omega}\frac{\cosh k(h+z)}{\cosh kh}\sin(kx-\omega t) \tag{3}$$

$$\omega^2 = gk\tanh kh \tag{4}$$

where k is the wavenumber, H is the wave height, h is the depth of the flow fluid, ω is the angular frequency of the wave, x and z are the coordinates of the point.

$$f = C_m \rho D^2 \dot{u} + \frac{1}{2} C_D \rho D |u + U|(u + U) \tag{5}$$

$$f = C_m \rho D^2 (\dot{U} - \ddot{x}) + \frac{1}{2} C_D \rho D |u + U - \dot{x}|(u + U - \dot{x}) \tag{6}$$

where f is the hydrodynamic force per length, C_m is the inertia coefficient, C_D is the drag coefficient, ρ is the density of the sea water, D is the diameter of the slender structure, U and $\dot{U}$ are the velocity and acceleration of the water particle, u is the current velocity, and $\dot{x}$ and $\ddot{x}$ are the velocity and acceleration of the structure element.

2.3. Convergence Analysis

A convergence analysis was done to identify the quality of the mesh. The model used in the convergence analysis was a fish cage with a height of 7 m, a diameter of 6 m under a current speed 0.5 m/s, wave period 10 s, and 1-m height. Four mesh models: course, medium, fine, and very fine were used. Number of elements and degrees of freedom are shown in Table 2. It also includes the maximum and minimum element lengths of each mesh model.

Table 2. Models and results of the convergence analysis.

Mesh Model	Course	Medium	Fine	Very Fine
Total nodes	322	842	1642	2162
Total elements	602	1122	1922	2442
Degrees of freedom,	1200	2760	5160	6720
Max element length (mm)	1000	500	250	200
Min element length (mm)	471.2	235.6	157.1	117.8
Calculated amplitude of horizontal displacement (mm)	0.934	0.937	0.941	0.942

From the calculated results, the amplitude of the horizontal displacement from the fine mode was 0.941 m, which was 99.89% of the one from the very fine model. However, the very fine model had 27.1% more elements and 30.2% more degrees of freedom than the fine model, which makes the calculation time much longer. Thus, in order to ensure the accuracy and efficiency of the calculation at the same time, the fine model was used in the present calculation.

3. Analytical Model Formulation and Solution

The mathematical modelling of the floating flexible cylindrical net cage was formulated in a three-dimensional polar coordinate system (r, θ, z) being the axis of the cylinder cage at $r = 0$, with z- axis being vertically upward, and the fluid had an undisturbed free surface located at $z = 0$ in the water of finite depth h_2. The flexible cylinder is assumed to be surface-piercing, and the flexible net cage is modelled as a flexible porous membrane under uniform tensions of radius a and length h_1 having a porous membrane bottom of negligible thickness.

The fluid occupies the region $0 < r < \infty$, $-h_2 < z < 0$, except the cage. Hence, the fluid domain is divided into three regions—namely, R_1: $(-h_2 \leq z \leq 0,\ r \geq a)$, R_2: $(-h_1 \leq z \leq 0,\ r \leq a)$, and R_3: $(-h_2 \leq z \leq -h_1,\ r \leq a)$. Further, the notations S and G represent the submerged and the gap parts of the flexible net cage, respectively. The cylindrical flexible cage is connected by mooring lines with stiffness k_s at $r = a$, with $y = h_2$ being the bottom bed (see Figure 1). It is also assumed that there is a uniform current flowing with speed u making an angle θ with positive direction of the x- axis; hence, the components of current are $(u_1, u_2) = (u \cos\theta, u \sin\theta)$. Further, it is assumed that the fluid

is inviscid, incompressible, and the flow is irrotational and simply harmonic in time with the angular frequency ω.

Thus, there exist velocity potentials $\Phi_j(r,\theta,z,t)$, such that $\Phi_j(r,\theta,z,t) = u_1 x + u_2 y + \Phi_j(r,\theta,z,t)$, j = 1,2,3.

The velocity potentials $\Phi_j(r,\theta,z,t)$ satisfy the Laplace equation:

$$\left(\frac{\partial^2}{\partial r^2} + \frac{1}{r}\frac{\partial}{\partial r} + \frac{1}{r^2}\frac{\partial}{\partial \theta^2}\right)\Phi_j + \frac{\partial^2 \Phi_j}{\partial z^2} = 0 \text{ in the fluid domain,} \tag{7}$$

where r is the radial distance from the z-axis, and θ is the angle about the $x-$ axis.

The linearised free surface condition on $z = 0$ is given by

$$\left(\frac{\partial}{\partial t} + u_1\frac{\partial}{\partial x} + u_2\frac{\partial}{\partial y}\right)^2 \Phi_j + g\frac{\partial \Phi_j}{\partial z} = 0 \text{ for } j = 1,2 \tag{8}$$

where g is the acceleration due to gravity.

As the bottom is rigid, the bottom boundary condition yields

$$\frac{\partial \Phi_j}{\partial z} = 0 \text{ for } j = 1,3 \text{ on } z = -h_2. \tag{9}$$

Assuming that flexible porous membrane bed of the net cage satisfies Darcy's law for flow past a porous structure, the linearised kinematic boundary condition with a uniform current yields

$$\frac{\partial \Phi_2}{\partial z} = \frac{\partial \Phi_3}{\partial z} = \frac{\partial \eta}{\partial t} + u_1\frac{\partial \eta}{\partial x} + u_2\frac{\partial \eta}{\partial y} + ik_0 G(\Phi_3 - \Phi_2) \text{at } z = -h_1, \tag{10}$$

where k_0 is the wavenumber of the plane gravity wave. It may be noted that, if $u_1 = 0$ and $u_2 = 0$, then the reduced boundary condition in Equation (10) will be same as in [33,34].

Now, the dynamic condition on the submerged flexible porous membrane satisfies

$$\left(-T_f \nabla^2_{r\theta} + m_m \frac{\partial}{\partial t^2}\right)\eta = -\{P_3(r,\theta,z,t) - P_2(r,\theta,z,t)\}, \tag{11}$$

where $\eta(r,\theta,t) = \mathrm{Re}\{\varsigma(r,\theta)e^{i\omega t}\}$ is the deflection of the flexible porous membrane bed, which is under the action of a uniform tensile force T_f, m_m is the mass of the membrane, and the hydrodynamic pressure in the presence of current can be read as

$$P_j(x,y,z,t) = \rho g z - \rho\left(\frac{\partial}{\partial t} + u_1\frac{\partial}{\partial x} + u_2\frac{\partial}{\partial y}\right)\Phi_j \text{ for } j = 2,3 \tag{12}$$

Next, it is assumed that the horizontal deflection of the vertical porous membrane of the cage is given by $\xi(z,t) = \mathrm{Re}\{\zeta(z)e^{i\omega t}\}$. Hence, the linearised kinematic condition on the vertical boundary of the cage at $r = a, z \in S$ is obtained as

$$\frac{\partial \Phi_j}{\partial r} = ik_0(\Phi_2 - \Phi_1) + \left(\frac{\partial}{\partial t} + u_1\frac{\partial}{\partial x} + u_2\frac{\partial}{\partial y}\right)\xi\cos\theta \text{ for } j = 1,2 \tag{13}$$

with k_0 being the same as in Equation (10). Further, the membrane deflection $\xi(z,t)$ at $r = a, z \in S$ satisfies the linearised dynamic conditions:

$$\left(m_m\frac{d^2}{dt^2} - T_g\frac{d^2}{dz^2}\right)\xi = 2a\rho\int_0^\pi \left(\frac{\partial \Phi_2}{\partial t} - \frac{\partial \Phi_1}{\partial t}\right)\cos(\pi - \theta)d\theta, \tag{14}$$

where T_g is the uniform tensile force acting on the vertical membrane of the cage.

In order to avoid structural failures in storm waves and currents during storm events, the net cages can be submerged below the water surface. Therefore, it is assumed that the cylindrical net cage is connected with mooring lines with stiffness k_s over the circumference of the cylinder ($r = a$), which gives (as in [32,34])

$$T_f \frac{\partial \xi}{\partial z} = k_s \xi \text{ at } r = a,\ z = 0 \tag{15}$$

On the other hand, it is considered that the cylindrical cage is fixed at $z = -h_1$, which implies

$$\xi(z,t) = 0 \text{at } z = -h_1,\ r = a \tag{16}$$

Further, it is assumed that the flexible porous membrane is fixed at the circumference and yields

$$\varsigma(r,\theta,z) = 0 \text{at } r = a,\ z = -h_1 \tag{17}$$

The continuity of the pressure and normal velocity at the interface $r = a$ yield

$$\Phi_1 = \Phi_3 \text{ at } r = a, z \in G \tag{18}$$

$$\frac{\partial \Phi_1}{\partial r} = \frac{\partial \Phi_3}{\partial r} \text{ at } r = a, z \in G, \tag{19}$$

Finally, the velocity potential in R_1 satisfies the radiation boundary it is given by (as in [42])

$$\lim_{r\to\infty} \sqrt{r}\left(\frac{\partial \Phi_1}{\partial r} + ik_0\Phi_1\right) = 0 \tag{20}$$

In the next section, the solution procedure in terms of the spatial components of the velocity potentials and horizontal displacement will be discussed.

Analytical Solution

Using the Fourier-Bessel series expansion formula, the velocity potentials satisfying governing Equation (8), along with the relevant boundary conditions in Equations (8)–(10), (15), and (20) in their respective regions, the velocity potentials in R_1, R_2, and R_3 are derived as

$$\phi_1 = \frac{-ig}{2(\omega - uk_0)} g_0(z) \sum_{m=0}^{\infty} \alpha_m \left\{ J_m(k_0 r) + A_{m0} H_m^{(1)}(k_0 r) \right\} \cos m\theta + \sum_{m=0}^{\infty}\sum_{n=1}^{\infty} \alpha_m A_{mn} K_m(k_n r) g_n(z) \cos m\theta \tag{21}$$

$$\phi_2 = \frac{-ig}{2(\omega - up_n)} \sum_{m=0}^{\infty}\sum_{n=0}^{\infty} B_{mn}\alpha_m I_m(p_n r)\Psi_2(z)\cos m\theta, \tag{22}$$

$$\phi_3 = \frac{-ig}{2(\omega - up_n)} \sum_{m=0}^{\infty}\sum_{n=0}^{\infty} C_{mn}\alpha_m I_m(p_n r)\Psi_3(z)\cos m\theta, \tag{23}$$

where $\alpha_m = e^{im\pi/2}\varepsilon_m$, with $\varepsilon_m = \begin{cases} 1, \text{ for } m = 0 \\ 2, \text{ for } m \geq 1 \end{cases}$, $J_m(k_0 r)$, and $H_m(k_0 r)$ as the Bessel function and Hankel function of first kind of order m, respectively; $K_m(k_0 r)$ is the modified Bessel functions of the first kind of order m (as in [42]); and the eigenfunctions associated with the velocity potentials in Equations (21)–(23) are given by

$$g_n(z) = \begin{cases} \frac{\cosh k_n(z+h_2)}{\cosh k_n h_2}, n = 0 \\ \frac{\cos k_n(z+h_2)}{\cos k_n h_2}, n \geq 1 \end{cases} \Psi_2(z) = \frac{(\omega^2 \tanh p_n z + g p_n)\cosh p_n z}{(\omega^2 - g p_n \tanh p_n h_1)\cosh p_n h_1}, \Psi_3(z) = \frac{\cosh p_n(z+h_2)}{\sinh p_n(h_2 - h_1)},$$

with the wavenumbers k_n and p_n satisfying the dispersion relations as

$$(\omega - uk_n)^2 = g k_n \tanh k_n h_2 \tag{24}$$

and p_n satisfies the complex dispersion relation associated with the current and tensile force as

$$\begin{array}{l}\left\{(T_f p_n^2 - m_s)igk_0G - (\omega - up_n)2\right\}\{gp_n\tanh p_nH - (\omega - up_n)2\}\cosh p_nH \\ -p_n(T_f p_n^2 - m_s)\sinh p_n(H-h)\{p_n\tanh p_nh - (\omega - up_n)2\}\cosh p_nh = 0\end{array} \quad (25)$$

It may be noted that the roots k_n satisfy the dispersion relation (Equation (24)). Further, the root k_n for $n = 0$ is the real positive root that corresponds to the progressive waves, and the roots k_n for $n = 1, 2, 3, \ldots$ are the infinite imaginary roots that correspond to the evanescent waves.

In the gap region (G) and cage region (S): the following series relations give

$$\sum_{n=0}^{\infty} A_{1n}Y_{an}(z) + \sum_{q=0}^{\infty} C_{1q}Y_{cq}(z) + Y_0(z) = 0, z \in G, \quad (26)$$

$$\sum_{n=0}^{\infty} A_{1n}Z_{an}(z) + \sum_{q=0}^{\infty} C_{1q}Z_{cq}(z) + Z_0(z) = 0, z \in G. \quad (27)$$

$$\sum_{n=0}^{\infty} A_{1n}W_{an}(z) + \sum_{q=0}^{\infty} B_{1q}W_{bq}(z) + W_0(z) = 0, z \in S, \quad (28)$$

$$\sum_{n=0}^{\infty} A_{1n}X_{an}(z) + \sum_{q=0}^{\infty} B_{1q}X_{bq}(z) + X_0(z) = 0, z \in S, \quad (29)$$

where the expressions $Y_0, Z_0, W_0, X_0, Y_{an}, Z_{an}, W_{an}, X_{an}, Y_{cq}, Z_{cq}, W_{bq}$, and X_{bq} are associated with the Hankel, Bessel, and modified Bessel functions. In order to reduce these dual series relations to the system of linear equations by the least-squares approximation method, the series relations in Equations (17)–(20) are expressed as

$$\Gamma_{N,M}(z) = \sum_{n=0}^{N} A_{1n}V_{an}(z) + \sum_{q=0}^{M} B_{1q}V_{bq}(z) + \sum_{q=0}^{M} C_{1q}V_{cq}(z) + V_0(z) = 0. \quad (30)$$

Again, using the least-squares approximation method, Equation (30) yields (as in [43])

$$\int_{-h_2}^{0} |\Gamma_{N,M}(z)|^2 dz = \text{minimum}. \quad (31)$$

The set of unknown A_{1n}s is chosen to minimise the integral in Equation (31), which yields

$$\int_{-h_2}^{0} \overline{\Gamma}_{N,M}(z)\frac{\partial \Gamma_{N,M}(z)}{\partial A_{1n}} dz = 0, \quad (32)$$

where "-" denotes the complex conjugates. The functions V_{an}, V_{bq}, V_{cq}, and V_0 are associated with the Hankel function, Bessel function, and modified Bessel function in the gap and the submerged region, along with their respective eigenfunctions.

Similarly, another four systems of equations can be obtained: two equations are the combination of Equations (26)–(29). The other two are obtained from the moored edge condition as in Equation (15) and fixed edge condition as in Equation (16). Now, there are 4M + 5 equations and 4M + 5 unknowns, which will be solved numerically using the MATLAB code along with the Bessel, Hankel, and modified Bessel functions of second kind order to solve the systems Equations (26)–(29) and the equations from the moored edge and fixed edge conditions using built-in subroutine MATLAB to present the numerical results. Once the unknown coefficients associated with the velocity potentials are obtained, the horizontal displacement $\zeta(z)$ of the vertical flexible cylindrical cage can be obtained

by substituting ϕ_1 and ϕ_2 into Equation (14) and applying the partial differential equation solution method as

$$\zeta(z) = A\frac{\cos\lambda z}{\cos\lambda h} + B\frac{\sin\lambda z}{\sin\lambda h} + h_0 g_0(z) + \sum_{n=0}^{N} A_{1n}\Theta_{an} g_n(z) + \sum_{q=0}^{M} B_{bq}\Theta_{bq} p_q \Psi_2(z), \quad (33)$$

where $\lambda = (\omega\sqrt{m_m})$, and the expressions Θ_{an} and Θ_{bq} are associated with the Hankel function, Bessel function, and modified Bessel function.

4. Numerical Results and Discussions

In this section, the numerical results from the FEA and analytical model of the horizontal displacement of the flexible cylindrical net cage in the presence of a current are compared for different mooring stiffness, heights of the cage, and radii of the cage to check the accuracy of the FEA model. The effects of different current speeds and times on the cage shape deformations are analysed. Further, the axial loads on the mooring force for different design parameters are also investigated based on the FEA. Hereafter, all numerical computations are executed by considering the fluid density $\rho = 1025$ kgm^{-3} and acceleration due to gravity $g = 9.8$ ms^{-2}, unless mentioned otherwise. It may be noted that the numerical simulation for the FEA was performed on a laptop with an Intel® core i7-6700HQ CPU with a 2.6 GHz processor and 16 GB of installed ram memory. The average time required for each run was approximately 24 h. On the other hand, for the analytical computations, MATLABR2016b, 64-bit (win64) was used to perform calculations. All numerical computations from the analytical solution were performed on a desktop machine with an Intel ® core i7-4790 CPU with a 3.60 GHz processor and 8 GB of ram memory. On average, each case took roughly 7–10 min to finish.

4.1. Comparison of Numerical FEA Model Simulations against Analytical Solution

In this subsection, the numerical FEA model simulations are compared with the analytical model results in order to check the accuracy of the numerical model based on the FEA associated with the wave interaction with a moored flexible cylindrical net cage in the presence of a current. It may be mentioned that, as the horizontal displacements are important for engineering design and operation, in the present work, the FEA simulations for both are compared with the analytical results for different design parameters.

In Figure 2, the effects of different values of mooring stiffness on the cage horizontal displacement between the FEA numerical simulations and analytical results are compared versus time t(s) for water depth (h_2) = 50 m, cage radius (a) = 3 m, and cage height (h_1) = 7 m, and the other parametric values are the same as defined in Table 1. It is observed that the results of the horizontal displacement of the cage decrease with an increase in the values of mooring stiffness in both models. This shows that, with the increase in the mooring line stiffness, the floating cylindrical cage becomes more stable, and as a result, the displacement decreases. Further, it is found that the displacement between the FEA numerical model simulations and analytical results are in good agreement with respect to the same values of mooring stiffness.

From the comparison of the results (Figure 2), it is seen that the horizontal displacement profiles are similar, and the peak wave amplitudes are close in both models. It is again observed that the crest of the displacement is almost the same between the models with respect to their mooring stiffness, but the throughput of the displacement is more pronounced in the FEA model for both mooring stiffness. When the stiffness is 10^3 Nm^{-1}, the amplitudes of the horizontal displacement from the FEA model and analytical model are 0.941 m and 0.981 m, respectively. However, when the mooring stiffness decreases to 100 N/m, the amplitudes of the horizontal displacement from the FEA model and analytical model increase to 1.141 m and 1.098 m, respectively. From the point of view of the FEA model, this suggests that the present differences are mainly connected to a sinker and

nonlinear springs; therefore, the FEA model reproduces a higher crest/throughput of the displacement, with a higher mooring stiffness that the analytical model cannot reproduce.

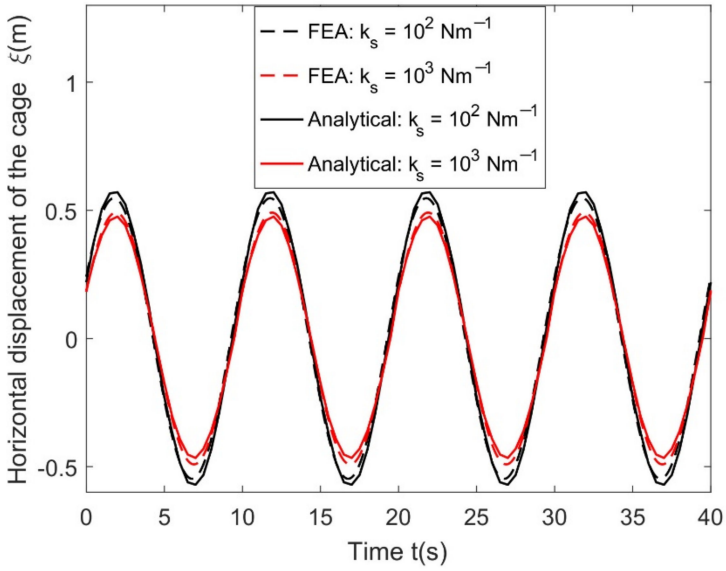

Figure 2. Comparison of the horizontal displacement of a cylindrical flexible cage for different mooring stiffness k_s between the numerical finite element analysis (FEA) and analytical simulations with $h_2 = 50$ m, $h_1 = 7$ m, and $a = 5$ m.

Figure 3 compares the horizontal displacement of the cylindrical flexible net cage for different cage heights between the FEA simulations and analytical results with $h_2 = 7$ m, $k_s = 10^3$ Nm^{-1}, and the other parametric values are the same as defined in Table 1 versus time t *(s)*. From comparing the results, it is seen that the effects of the cage height on the horizontal displacements are similar, and the peak values are in good agreement in both models. When the ratio between the cage height and water depth is 0.3, the amplitude of the horizontal displacement from the FEA model is 0.903 m, which is 0.8% lower than the one from the analytical model. When the ratio increases to 0.4, the amplitude of the horizontal displacement from the FEA model is 0.826 m, which is 2% higher than the one from the analytical model. Further, it is found that, as the cage height increases, the horizontal displacement increases, which suggests that, for taller structures, the horizontal displacement becomes more with certain values of the current speed and mooring stiffness.

In Figure 3, it is also observed that the phase shift occurs in the horizontal displacement, which is because of the interaction of the wave–current with the cage height changes, which leads to the constructive/destructive interference of waves at the edges of the cylindrical cage. Further, it may be explained that a part of the wave energy dissipates while passing through the porous net cage, and another part of the energy is used to deform the flexible net cage with a current, which plays an important role for constructive/destructive interference.

Figure 4 shows the comparisons of horizontal displacement between the numerical FEA simulations and analytical results for different radii of the cage versus time $t(\mathrm{s})$ with the same values of parameters: water depth $h_1 = 50$ m, cage height $h_2 = 7$ m, and mooring stiffness $k_s = 10^3$ Nm^{-1}. From Figure 4, it is observed that, as the radius a of the cage increases, the horizontal displacement of the cage increases. From the FEA model, the amplitude of the horizontal displacement of the cage with a diameter of 3 m is 0.942 m, which is 6.4% lower than the one of the cage with a diameter of 5 m. Meanwhile, from the analytical mode, the amplitude of horizontal displacement of the cage with a diameter of 3 m is 0.927 m, which is 6.1% lower than the one of the cage with a diameter of 5 m. This is

due to the fact that the area of the cage increases, and consequently, the area exposed to the wave loads increases.

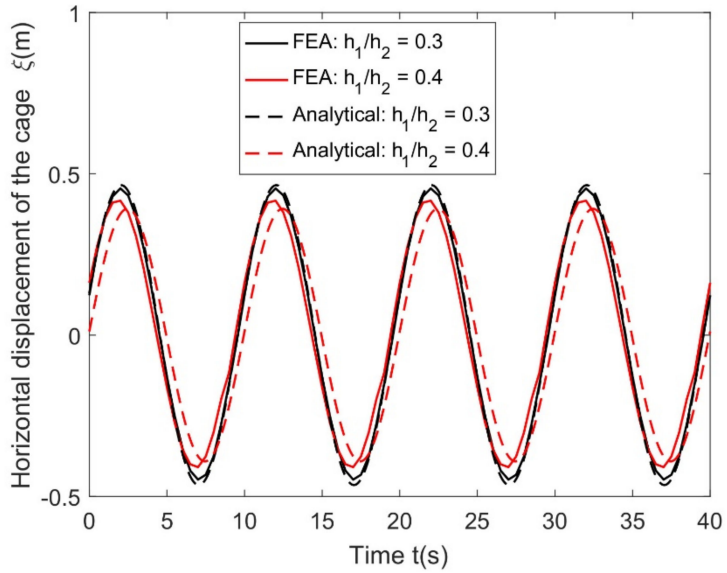

Figure 3. Comparison of the horizontal displacement of the cylindrical flexible net cage for a different cage height h_1 between the numerical FEA and analytical simulations for $h_2 = 50$ m, $a = 3$ m, and $k_s = 10^3$ Nm^{-1}.

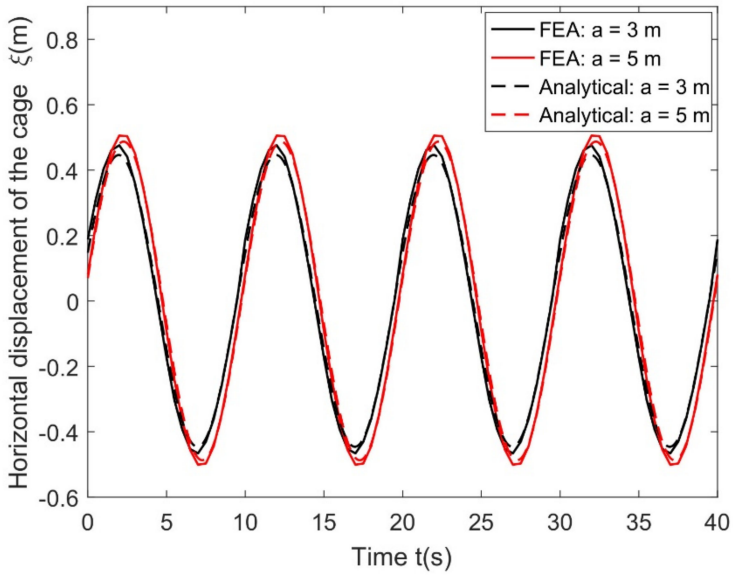

Figure 4. Comparison of the horizontal displacements for different cage radii a between the numerical FEA simulations and analytical results with $h_2 = 50$ m, $h_1 = 7$ m, $k_s = 10^3$ Nm^{-1}, and the other parametric values are the same as defined in Table 1.

To further validate the FEA analysis of the flexible net cage in the presence of a uniform current, the effects of flexible cage deformations and the axial loads due to waves on the mooring lines on different currents and times are investigated.

4.2. FEA Model Simulations for Different Design Parameters

In this subsection, the dynamic analysis of the net cage system is performed with the FEA, with the focus on the mooring loads due to the actions of the waves—more specifically,

the axial force, T [N]—and the deformation of the cage. Following the methodology of this work, the effects of varying parameters will be studied.

Figure 5 depicts the cage deformations for different current speeds of 0.2 m/s–1.2 m/s, with other parametric values defined in Table 1. It is observed that the deformation of the flexible net increases with the current speed. The collar does not deform much due to its high stiffness. The larger current provided larger hydrodynamic forces, which results in a larger horizontal deformation and lower height of the cage. Therefore, the volume of the cage reduces rapidly under a large current. The observations of the cage deformations under the current are similar to [9,11,28]. The blue lines are spring elements that represent the mooring system. The compression stiffness of the spring is set to zero, so there is no force from the downstream mooring, even if it is compressed.

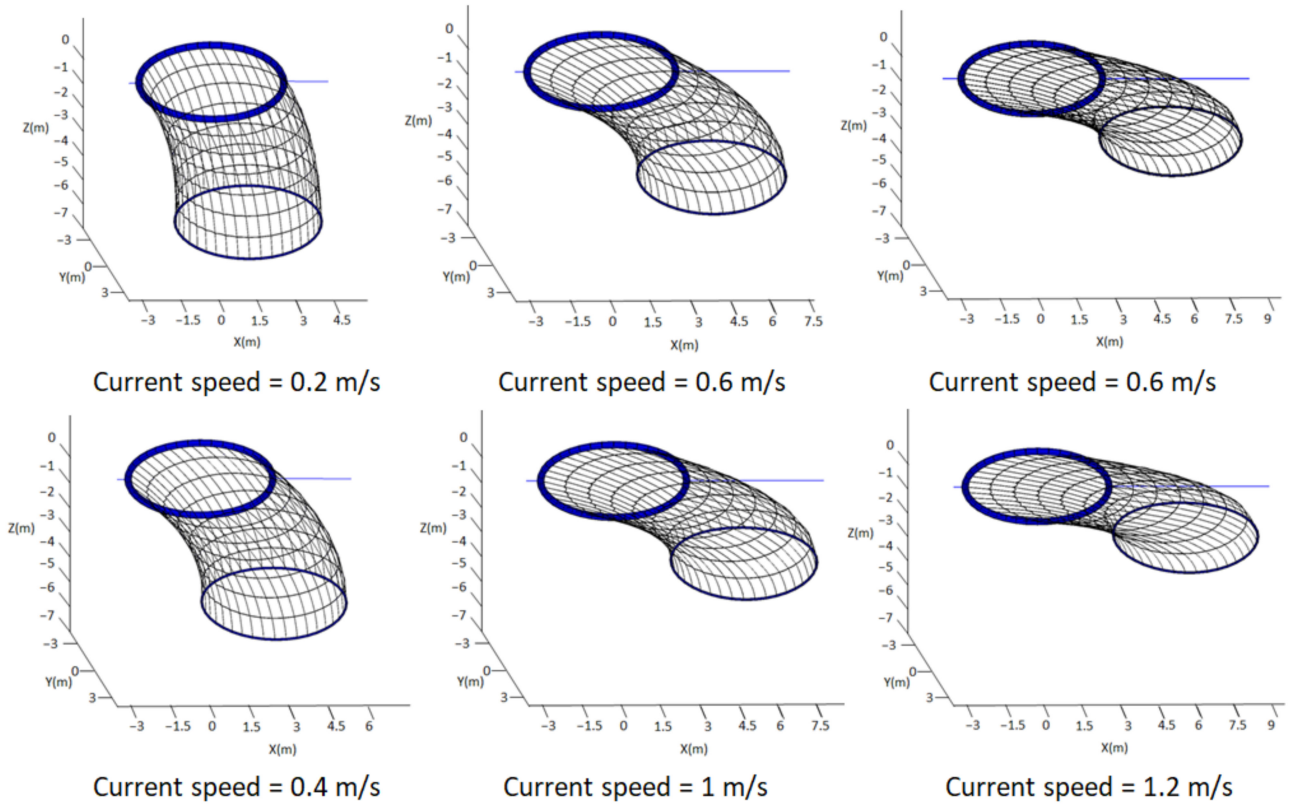

Figure 5. Variations of different current speeds on the cage displacements with a wave height = 1 m and wave period = 10 s, and the other parametric values are the same as mentioned in Table 1.

Figure 6 shows the shapes of the cage at different moments in one period when the current speed is 0.5 m/s, the wave height is 1 m, and the wave period is 10 s under the effect of both the current and waves. The general observations are similar as in Figure 5. However, the deformation of the net varies slightly during one period, so the shape and the volume of the cage do not change much. Further, it can be observed that the motion of the cage is close to the motion of the wave, so it is hard to tell the differences between the shapes of the cage under different times in one period, especially when it is a 3D view. However, some differences can be seen after scales are added and the view direction is adjusted. In Figure 6, firstly, the tilt angles of the collar and the bottom ring vary. Secondly, the height of the cage also varies. The cage does approximate a rigid motion with wave fluctuation. The deformation and mooring force under different currents and waves are also studied in [12,15].

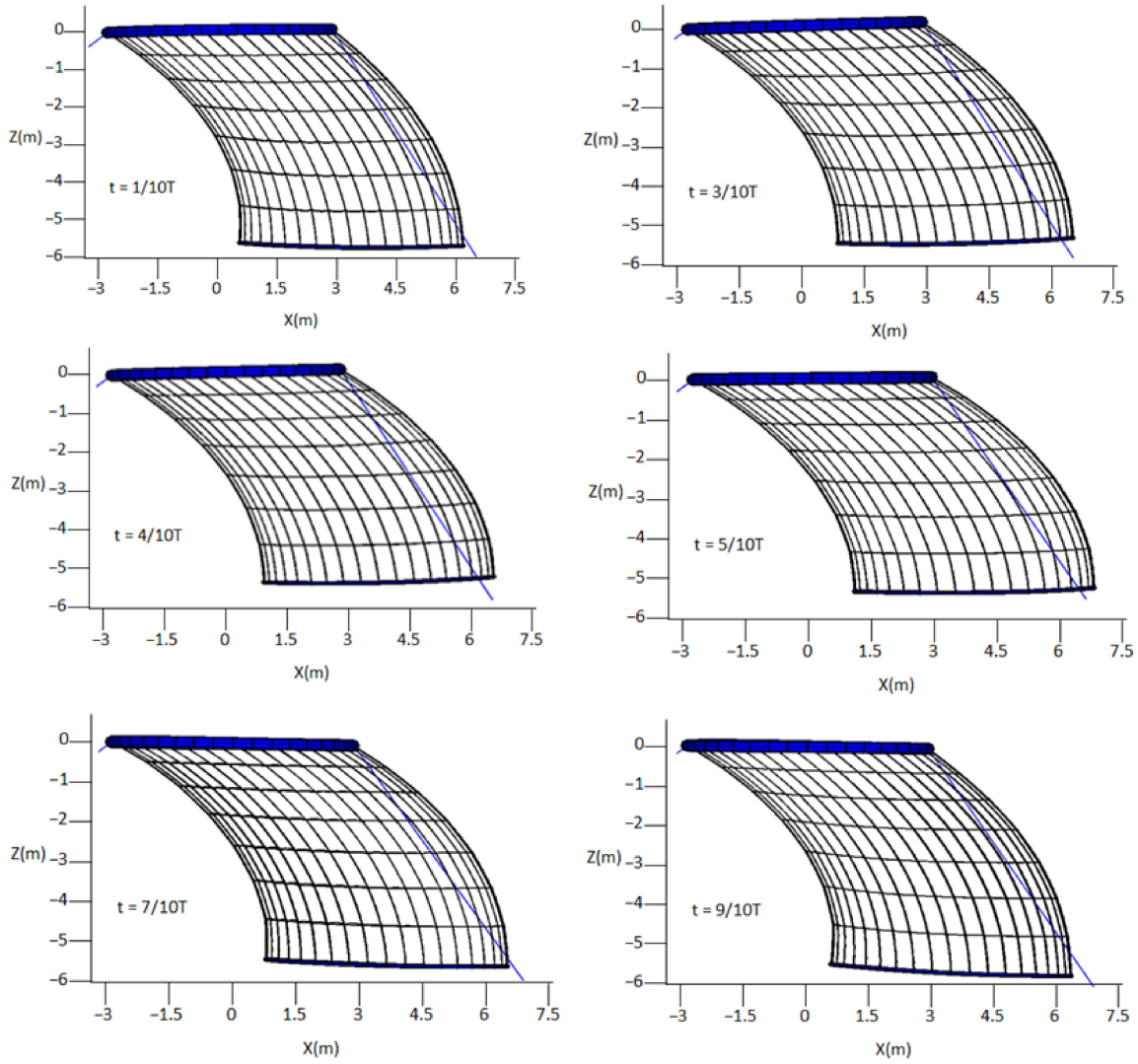

Figure 6. Cage deformation representing the net deformation for different times with a wave height = 1 m, wave period = 10 s, and current speed $u = 0.5$ m$/s$, and the other parametric values are the same as defined in Table 1.

In Figure 7, the effects of the mooring force on the different cage radii versus time with water depth $h_2 = 50$ m, cage height $h_1 = 7$ m, and $u = 0.5$ ms^{-1} are plotted. It is observed that the force on the structure increases with an increase in the cage radius. This is due to the fact that the cage with a larger radius has a larger projected area under the current, which results in a larger hydrodynamic force and mooring force. On the other hand, from Figure 8, the amplitudes of the mooring forces are very close, which confirms the results of the displacements in Figure 4.

In Figure 8, the effects of different cage heights on the mooring force versus time t(s) with a water depth $h_2 = 50$ m, $k_s = 10^3$ Nm^{-1}, and $u = 0.5$ m/s are plotted. It is observed that mooring force increases with an increase in cage height, which is due to the area of the cylindrical cage increasing, and consequently, the area exposed to the wave loads increasing.

It may be mentioned that, if the static forces are removed from Figures 7 and 8, readers may be confused, as the values of the mooring forces are important, because they show that larger cages under the same sea conditions can result in larger mooring forces.

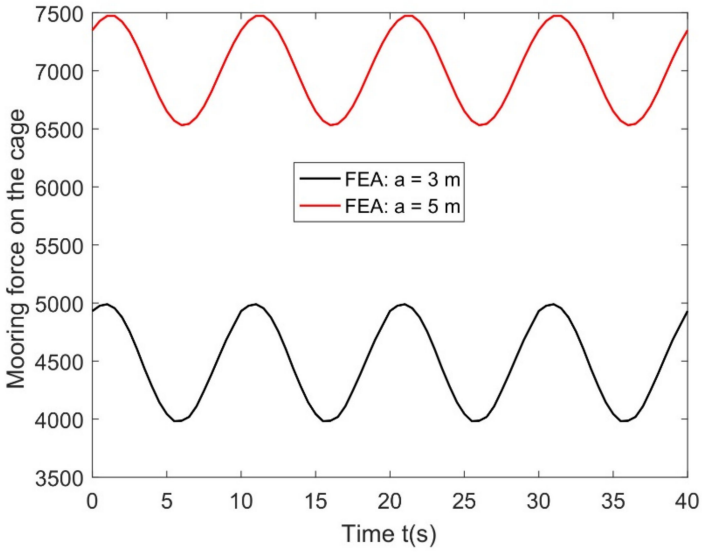

Figure 7. Effects of the cage radius on the mooring force versus time t(s) with a water depth $h_1 = 50$ m, cage height $h_2 = 7$ m, and $u = 0.5$ m/s.

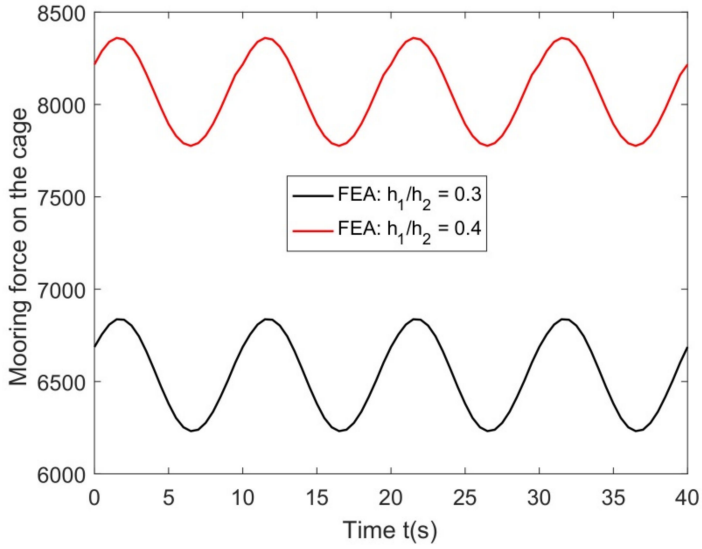

Figure 8. Effects of different cage heights h_1 versus time t(s) for a water depth $h_1 = 50$ m, $k_s = 10^3$ Nm^{-1}, and current speed $u = 0.5$ m/s.

5. Conclusions

In the present paper, a numerical model based on the FEA and an analytical model under the potential flow theory associated with a moored flexible cylindrical net cage in the presence of a current were presented. The results of horizontal displacement under the current velocity between the two models were compared for different design parameters. Further, the results of the cage deformations and mooring forces for different design parameters were analysed from the FEA simulations. It was concluded that:

1. The numerical simulations of the horizontal displacements for different design parameters of the flexible net cage were in good agreement with the analytical model results.
2. As the current speed, cage height, and diameter of the cage increased, the horizontal displacement increased. This was because the projected area of the cage increased, which looked physically reasonable.
3. The analysis of the 3D cage displacements for different current speeds suggested that the cylindrical cage became more stable for lower values of the current speed.

4. The increase of the height and radius enlarged the mooring force, because it increased the projected area of the cage.
5. Comparisons of the results confirming that the developed numerical model based on the FEA might be useful to study the dynamics response of flexible fishing net systems.

Author Contributions: Conceptualisation of the problem was developed by Z.L., S.C.M. and C.G.S. The FEA analysis was performed by Z.L., and the analytical model analysis was performed by S.C.M. The writing of the original draft manuscript was done by Z.L., S.C.M. and C.G.S. All authors have read and agreed to the published version of the manuscript.

Funding: This work was performed within the project HYDROELASTWEB—Hydroelastic behaviour of horizontal flexible floating structures for applications to Floating Breakwaters and Wave Energy Converters, which was funded by the Portuguese Foundation for Science and Technology (Fundação para a Ciência e a Tecnologia—FCT) under contract 031488_770 (PTDC/ECI-EGC/31488/2017). The first author was funded by the Portuguese Foundation for Science and Technology (Fundação para a Ciência e a Tecnologia-FCT) through a doctoral fellowship under contract no. SFRH/BD/147178/2019. The second author was contracted as a Researcher by the Portuguese Foundation for Science and Technology (Fundação para a Ciência e Tecnologia-FCT) through the Scientific Employment Stimulus individual support under contract no. CEECIND/04879/2017. This work contributed to the Strategic Research Plan of the Centre for Marine Technology and Ocean Engineering (CENTEC), which was financed by the Portuguese Foundation for Science and Technology (Fundação para a Ciência e Tecnologia—FCT) under contract UIDB/UIDP/00134/2020.

Institutional Review Board Statement: Not applicable.

Informed Consent Statement: Not applicable.

Data Availability Statement: Not applicable.

Conflicts of Interest: The authors declare no conflict of interest.

Abbreviations

APDL	ANSYS Parametric Design Language
CFD	Computational Fluid Dynamics
CIP	Carbon-in-Pulp
FEA	Finite Element Analysis
FEM	Finite Element Method
HDPE	High Density Polyethylene
NWT	Numerical Wave Tank

References

1. He, Z.; Faltinsen, O.M.; Fredheim, A.; Kristiansen, T. The influence of fish on the mooring loads of a floating net cage. *J. Fluids Struct.* **2018**, *76*, 384–395. [CrossRef]
2. Shen, Y.; Greco, M.; Faltinsen, O.M.; Nygaard, I. Numerical and experimental investigations on mooring loads of a marine fish farm in waves and current. *J. Fluids Struct.* **2018**, *79*, 115–136. [CrossRef]
3. Faltinsen, O.M.; Shen, Y. Wave and current effects on floating fish farms. *J. Mar. Sci. Appl.* **2018**, *17*, 284–296. [CrossRef]
4. Holmer, M. Environmental issues of fish farming in offshore waters: Perspectives, concerns and research needs. *Aquac. Environ. Interact.* **2010**, *1*, 57–70. [CrossRef]
5. Benetti, D.D.; Benetti, G.I.; Rivera, J.A.; Sardenberg, B.; O'Hanlon, B. Site Selection Criteria for Open Ocean Aquaculture. *Mar. Technol. Soc. J.* **2010**, *44*, 22–35. [CrossRef]
6. Lee, C.W.; Kim, H.S.; Lee, G.H.; Koo, K.Y.; Choe, M.Y.; Cha, B.J.; Jeong, S.J. Computation modeling of the moored flexible structures. In *Maritime Transportation and Exploitation of Ocean and Coastal Resources*; Guedes Soares, C., Garbatov, Y., Fonseca, N., Eds.; Taylor & Francis Group: London, UK, 2005; pp. 1239–1243.
7. Moe, H.; Fredheim, A.; Hopperstad, O.S. Structural analysis of aquaculture net cages in current. *J. Fluids Struct.* **2010**, *26*, 503–516. [CrossRef]
8. Moe-Føre, H.; Lader, P.; Lien, E.; Hopperstad, O. Structural response of high solidity net cage models in uniform flow. *J. Fluids Struct.* **2016**, *65*, 180–195. [CrossRef]
9. Lader, P.; Dempster, T.; Fredheim, A.; Jensen., F. Current induced net deformations in full-scale cages for Atlantic salmon (Salmo salar). *Aquac. Eng.* **2008**, *38*, 52–65. [CrossRef]

10. De Cew, J.; Fredriksson, D.W.; Lader, P.F.; Chambers, M.; Howell, W.H.; Osienki, M.; Celikkol, B.; Frank, K.; Høy, E. Field measurements of cage deformation using acoustic sensors. *Aquac. Eng.* **2013**, *57*, 114–125. [CrossRef]
11. Gansel, L.; Oppedal, F.; Birkevold, J.; Tuene, S. Drag forces and deformation of aquaculture cages-Full-scale towing tests in the field. *Aquac. Eng.* **2018**, *81*, 46–56. [CrossRef]
12. Bai, X.; Xu, T.; Zhao, Y.; Dong, G.; Bi, C. Fatigue assessment for the floating collar of a fish cage using the deterministic method in waves. *Aquac. Eng.* **2016**, *74*, 131–142. [CrossRef]
13. Berstad, A.J.; Tronstad, H. Response from current and regular/irregular waves on a typical polyethylene fish farm. In *Maritime Transportation and Exploitation of Ocean and Coastal Resources*; Guedes Soares, C., Garbatov, Y., Fonseca, N., Eds.; Taylor & Francis Group: London, UK, 2005; pp. 1189–1196.
14. Fu, S.; Xu, Y.; Hu, K.; Zhang, Y. Experimental investigation on hydrodynamics of floating cylinder in oscillatory and steady flows by forced oscillation test. *Mar. Struct.* **2013**, *34*, 41–55. [CrossRef]
15. Li, L.; Fu, S.; Xu, Y.; Wang, J.; Yang, J. Dynamic responses of floating fish cage in waves and current. *Ocean Eng.* **2013**, *72*, 297–303. [CrossRef]
16. Moe-Føre, H.; Christian, E.P.; Gunnar, A.K.; Jensen, J.; Føre, M.; Kristiansen, D.; Fredheim, A.; Lader, P.; Reite, K. Structural Analysis of Aquaculture Nets: Comparison and Validation of Different Numerical Modeling Approaches. *J. Offshore Mech. Arct. Eng.* **2015**, *137*, 041201. [CrossRef]
17. Moe, H.; Fredheim, A.; Heide, M.A. New net cage designs to prevent tearing during handling. In *Maritime Transportation and Exploitation of Ocean and Coastal Resources*; Guedes Soares, C., Garbatov, Y., Fonseca, N., Eds.; Taylor & Francis Group: London, UK, 2005; pp. 1265–1272.
18. Endresen, P.C.; Fore, M.; Fredheim, A.; Kristiansen, D.; Enerhaug, B. Numerical Modelling of Wake Effect on Aquaculture Nets. In Proceedings of the 32nd International Conference on Ocean, Offshore and Arctic Engineering, Nantes, France, 9–14 June 2013; ASME: New York, NY, USA, 2013. Paper No. OMAE2013-11446.
19. Gutiérrez-Romero, J.E.; Lorente-López, A.J.; Zamora-Parra, B. Numerical analysis of fish farm behaviour in real operational conditions. *Ships Offshore Struct.* **2019**, *15*, 737–752. [CrossRef]
20. Ma, L.; Hu, K.; Fu, S.; Moan, T.; Li, R. A hybrid empirical-numerical method for hydroelastic analysis of a floater-and-net system. *J. Ship Res.* **2016**, *60*, 14–29. [CrossRef]
21. Martin, T.; Tsarau, A.; Bihs, H. A numerical framework for modelling the dynamics of open ocean aquaculture structures in viscous fluids. *Appl. Ocean. Res.* **2020**, *106*, 102410. [CrossRef]
22. Kristiansen, D.; Faltinsen, O.M. Nonlinear wave induced motions of cylindrical-shaped floaters of fish farms. *Proc. Inst. Mech. Eng. Part M J. Eng. Marit. Environ* **2009**, *223*, 361–375.
23. Kristiansen, T.; Faltinsen, O.M. Mooring loads of a circular net cage with an elastic floater in waves and current. In Proceedings of the 6th International Conference om Hydroelasticity in Marine Technology, Tokyo, Japan, 19–21 September 2012; ClassNK: Tokyo, Japan, 2012; pp. 183–192.
24. Kristiansen, T.; Faltinsen, O.M. Modelling of current loads on aquaculture net cages. *J. Fluids Struct.* **2012**, *34*, 218–235. [CrossRef]
25. Kristiansen, T.; Faltinsen, O.M. Experimental and numerical study of an aquaculture net cage with floater in waves and current. *J. Fluids Struct.* **2015**, *54*, 1–26. [CrossRef]
26. Huang, C.C.; Tang, H.J.; Liu, J.Y. Effects of waves and currents on gravity-type cages in the open sea. *Aquac. Eng.* **2008**, *38*, 105–116. [CrossRef]
27. Xu, T.J.; Zhao, Y.P.; Dong, G.H.; Gui, F.K. Analysis of hydrodynamic behavior of a submersible net cage and mooring system in waves and current. *Appl. Ocean Res.* **2013**, *42*, 155–167. [CrossRef]
28. Xu, T.J.; Zhao, Y.P.; Dong, G.H.; Li, Y.C.; Gui, F.K. Analysis of hydrodynamic behaviors of multiple net cages in combined wave-current flow. *J. Fluids Struct.* **2013**, *39*, 222–236. [CrossRef]
29. Klebert, P.; Patursson, Ø.; Endresen, P.; Rundtop, P.; Birkevold, J.; Rasmussen, H. Three-dimensional deformation of a large circular flexible sea cage in high currents: Field experiment and modelling. *Ocean Eng.* **2015**, *104*, 511–520. [CrossRef]
30. Zhao, Y.P.; Bai, X.D.; Dong, G.H.; Bi, C.W. Deformation and stress distribution of floating collar of net cage in steady current. *Ships Offshore Struct.* **2019**, *14*, 371–383. [CrossRef]
31. Mohapatra, S.C.; Guedes Soares, C. Effect of submerged horizontal flexible membrane on moored floating elastic plate. In *Maritime Technology and Engineering 3*; Guedes Soares, C., Santos, T.A., Eds.; Taylor & Francis Group: London, UK, 2016; pp. 1181–1188.
32. Mohapatra, S.C.; Guedes Soares, C. Interaction of ocean waves with floating and submerged horizontal flexible structures in three-dimensions. *Appl. Ocean Res.* **2019**, *83*, 136–154. [CrossRef]
33. Mohapatra, S.C.; Guedes Soares, C. Hydroelastic response of a flexible submerged porous plate for wave energy absorption. *J. Mar. Sci. Eng.* **2020**, *8*, 698. [CrossRef]
34. Guo, Y.C.; Mohapatra, S.C.; Guedes Soares, C. Wave energy dissipation of a submerged horizontal flexible porous membrane under oblique wave interaction. *Appl. Ocean Res.* **2020**, *94*, 101948. [CrossRef]
35. Guo, Y.C.; Mohapatra, S.C.; Guedes Soares, C. Composite breakwater of a submerged horizontal flexible porous membrane with a lower rubble mound. *Appl. Ocean Res.* **2020**, *104*, 102371. [CrossRef]
36. Su, W.; Zhan, J.M.; Huang, H. Analysis of a porous and flexible cylinder in waves. *China Ocean Eng.* **2015**, *29*, 357–368. [CrossRef]
37. Guo, Y.C.; Mohapatra, S.C.; Guedes Soares, C. Review of developments in porous membranes and net-type structures for breakwaters and fish cages. *Ocean Eng.* **2020**, *200*, 107027. [CrossRef]

38. Endressen, C.; Birkevold, J.; Feae, M.; Fredheim, A.; Kristiansen, D.; Lader, P. Simulation and validation of a numerical model of a full aquaculture net-cage system. In Proceedings of the 33rd International Conference on Ocean., Offshore and Arctic Engineering, San Francisco, CA, USA, 8–13 June 2014; ASME: New York, NY, USA, 2014. Paper No: OMAE2014-23382, V007T05A006.
39. Fredheim, A. Current Forces on Net Structures. Ph.D. Thesis, NTNU, Trondheim, Norway, 2005.
40. Faltinsen., O.M. Viscous Wave Loads and Damping. In *Sea Loads on Ships and Offshore Structures*; Cambridge University Press: Cambridge, UK, 1990; pp. 223–226.
41. Xu, Z.; Qin, H. Fluid-structure interactions of cage-based aquaculture: From structures to organisms. *Ocean Eng.* **2020**, *217*, 107961. [CrossRef]
42. Mohapatra, S.C.; Islam, H.; Guedes Soares, C. Boussinesq Model and CFD Simulations of Non-Linear Wave Diffraction by a Floating Vertical Cylinder. *J. Mar. Sci. Eng.* **2020**, *8*, 575. [CrossRef]
43. Lee, W.K.; Lo, E.Y.M. Surface-penetrating flexible membrane wave barriers of finite draft. *Ocean Eng.* **2002**, *29*, 1781–1804. [CrossRef]